HHS Public Access

Author manuscript

Angew Chem Int Ed Engl. Author manuscript; available in PMC 2021 February 17.

Published in final edited form as:

Angew Chem Int Ed Engl. 2020 February 17; 59(8): 3209–3217. doi:10.1002/anie.201910828.

Dimethyl-dihydroacridines as Photocatalysts in the Organocatalyzed Atom Transfer Radical Polymerization of Acrylate Monomers

Bonnie L. Buss[a], **Chern-Hooi Lim**[a,b], **Garret M. Miyake**[a]

[a]Department of Chemistry, Colorado State University, Fort Collins, CO 80523, United States

[b]New Iridium LLC, Boulder, CO 80303, United States

Abstract

Development of photocatalysts (PCs) with diverse properties has been essential in advancement of organocatalyzed atom transfer radical polymerization (O-ATRP). In this work, dimethyl-dihydroacridines are presented as a new family of organic PCs, for the first time enabling controlled polymerization of challenging acrylate monomers via O-ATRP. Structure-property relationships for seven PCs are established, demonstrating tunable photochemical and electrochemical properties and accessing a strongly oxidizing $^{2}PC^{\bullet+}$ intermediate for efficient deactivation. In O-ATRP, a combination of PC choice, implementation of continuous-flow reactors, and promotion of deactivation through addition of LiBr are critical to producing well-defined acrylate polymers with dispersities as low as 1.12. The utility of this approach is established through demonstration of the oxygen tolerance of the system and application to diverse acrylate monomers, including the synthesis of well-defined di- and triblock copolymers.

Graphical Abstract

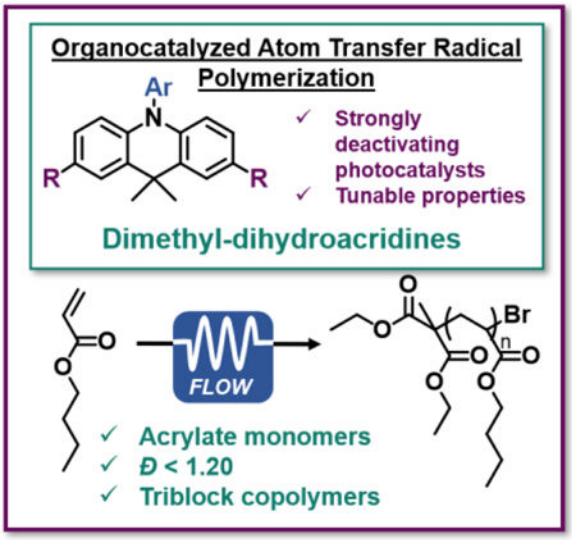

garret.miyake@colostate.edu.

Organic photoredox catalysis is applied to the controlled synthesis of poly(acrylates). This advancement is enabled by development of new organic photoredox catalysts with unique properties, as well as through application to continuous flow reactors.

Keywords

photoredox catalysis; polymerization; monomers; microreactors

Introduction

The ability of photoredox catalysis to manipulate electron or energy transfer reactivity has revolutionized small molecule and macromolecular chemistry, presenting opportunities to develop new chemical transformations under mild and energy efficient reaction conditions.[1] Recently, photoredox catalysis has been applied in controlled radical polymerization (CRP) approaches for light-regulated synthesis of well-defined polymers, most commonly in atom transfer radical polymerization (ATRP) and reversible addition-fragmentation transfer (RAFT).[2] ATRP, the most widely studied CRP methodology, is used to access polymers with controlled properties, higher-order architectures, and consequently diverse applications.[3] Traditionally, ATRP is operated through activation of a Cu(I) catalyst by heat to promote an inner-sphere electron transfer to generate a propagating radical species. However, in recent advances, new light-driven ATRP processes have been reported using photocatalysts (PCs) derived from copper, ruthenium, or iridium.[4]

Organocatalyzed atom transfer radical polymerization (O-ATRP) is a metal-free variant of photoredox-catalyzed ATRP which eliminates the concern of trace metal contamination in the polymer product and is advantageous in electronic and biomedical applications, while also enabling opportunities for “greener” reaction design in polymer synthesis.[5] Induced by light, O-ATRP relies on a strongly reducing organic PC to mediate an oxidative quenching catalytic cycle (Figure 1a). O-ATRP processes following a reductive quenching pathway have also been reported but rely on the presence of stoichiometric quantities of sacrificial electron donors, which can also induce undesirable side reactions.[6] The proposed O-ATRP mechanism proceeds through four central steps.[7] Photoexcitation of a ground-state PC generates ^{1}PC*, which can undergo intersystem crossing to produce a long-lived ^{3}PC*. Either ^{1}PC* or ^{3}PC* then directly reduces an alkyl halide initiator through outer-sphere electron transfer to produce a propagating radical species, as well as the ion-pair $^{2}PC^{\bullet+}X^{-}$. Deactivation of the propagating chain-end occurs through reinstallation of the halide, generating the PC and a dormant polymer. Central to success in O-ATRP, as determined by control over polymer molecular weight (MW) and dispersity (*Đ)* close to 1.0, is the presence of a dynamic equilibrium between the activation and deactivation steps, where the rate of deactivation (with rate constant k_d) must be higher than the rates of propagation (k_p) and activation (k_a), limiting radical concentrations and undesirable termination events via radical quenching.

To date, advances in O-ATRP have been enabled through development of strongly reducing organic PCs, which are capable of directly reducing an activated alkyl bromide ATRP

initiator or dormant polymer chain-end (~−0.8 V vs. SCE).[8] In 2014, perylene and *N*-phenyl phenothiazine were reported as strongly-reducing PCs for the polymerization of methacrylate monomers via O-ATRP.[9] Since then, other organic PCs derived from *N,N*-diaryl dihydrophenazine[10] and *N*-aryl phenoxazine[11] families, among others[12], have been developed (Figure 1b). *N*-aryl phenothiazine PCs have been applied in diverse contexts[13] and have also been used for mechanistic analysis[14]. Recently, PC structure-property relationships have been studied using *N,N*-diaryl dihydrophenazine and *N*-aryl phenoxazine PCs.[15] Empirically, these studies have determined key PC design principles for effective catalytic performance in O-ATRP, among which are the ability of the PC to exhibit intramolecular charge transfer (CT) excited states, redox reversibility, and sufficient thermodynamic driving forces (redox potentials) to mediate the oxidative quenching O-ATRP cycle.[16] *N,N*-diaryl dihydrophenazine and *N*-aryl phenoxazine PCs have also been studied in diverse polymerization-related contexts, including the effects of light intensity and solvent, adaptation of O-ATRP to continuous-flow reactors, synthesis of star polymers, and demonstration of oxygen tolerance.[17a-e] In addition, these organic PCs were also applied in small molecule reactions, including trifluoromethylation, C-N and C-S cross couplings via dual catalytic approach with Ni(II) salts, and the reduction of carbon dioxide to methane using sunlight for solar fuel generation.[17f-g]

Despite advances in PC design, O-ATRP has largely been limited to polymerization of methacrylate monomers, but the controlled polymerization of other monomers is highly desired.[18] Poly(acrylates) possess disparate thermal and mechanical properties, enabling widespread industrial and academic use, including drug delivery, superabsorbent materials, coatings, adhesives and additive manufacturing.[19] As such, we sought to leverage current understanding of organic PC design to target the O-ATRP of acrylate monomers. The CRP of acrylates is inherently challenging due to high k_p, with values ranging from 15,000 to 24,000 L $mol^{-1}s^{-1}$,[20] an order of magnitude larger than methacrylates. Furthermore, acrylate chain-end groups containing bromides are more difficult to reduce compared to the corresponding methacrylates, emphasizing the need for efficient PCs for activation.[x]

Photoinduced copper-catalyzed ATRP processes have been reported for successful CRP of acrylate monomers.[21] Additionally, a photoredox-catalyzed ATRP approach of acrylates was also performed using a precious metal-based *fac*-$Ir(ppy)_3$ PC following an oxidative quenching catalytic cycle, accessing control over MW growth to produce polymers with moderate *Đ*.[22] To access this polymerization with an organic PC, we hypothesized that a PC candidate must possess both a sufficiently oxidizing $^2PC^{\bullet+}$ with a correspondingly high $E_{1/2}$ ($^2PC^{\bullet+}/^1PC$) potential to promote fast deactivation (high k_d) to compensate for high k_p, but also maintain a strongly reducing $^3PC^*$ with sufficiently negative $E^0(^2PC^{\bullet+}/^3PC^*)$ value for efficient alkyl bromide activation.

Using density functional theory (DFT) calculations to guide organic PC design, herein dimethyl-dihydroacridines are reported as a new class of organic PCs adept at controlled polymerizations of acrylate monomers via O-ATRP. Due to structural similarity to previously employed PCs in O-ATRP and tunable donor-acceptor motifs, we sought to investigate this class of molecules for use in photoredox-catalyzed processes, accessing tailored photo- and electrochemical properties. In this approach, well-defined acrylate

polymers with controlled molecular weights and low dispersities ($Đ \leq 1.20$) were synthesized using a 365 nm LED in a continuous-flow reactor in conjuction with LiBr salt additives, which are hypothesized to promote efficient deactivation.

Results and Discussion

1. Photocatalyst Development

Dimethyl-dihydroacridines have previously been applied in the development of organic LEDs as thermally activated delayed fluorescence emitters. Tunable absorption profiles, small S_1 and T_1 energy gaps ($\Delta E_{ST} < 0.4$ eV), as well as CT characteristics were reported, [23] making this a promising structural motif for application in photoredox catalysis. Initial DFT calculations for 9,9-dimethyl-10-(naphthalen-1-yl)-9,10-dihydroacridine (**1a**) predicted an E^0_{ox} ($^2PC^{\bullet+}/^1PC$) value of 0.72 V vs. SCE. Corroborating DFT prediction, **1a** was experimentally determined to have an $E_{p/2}$ value of 0.82 V vs. SCE (Figure 2a). Although **1a** displayed a non-reversible cyclic voltammogram, this relatively high $E_{p/2}$ value encouraged further exploration of dimethyl-dihydroacridines as potential PC candidates, as current successful strongly-reducing PCs in O-ATRP only have $E_{1/2}$ up to ~ 0.7 V vs. SCE.[16]

Notably, installation of biphenyl groups at the 2 and 7 positions of **1a** imparted redox reversibility, a key requirement for catalyst turnover (Figure 2a). Furthermore, relative to **1a**, increasing the conjugation of the dimethyl-dihydroacridine molecules also red-shifted the absorption profile by ~80 nm, presenting the possible use of milder irradiation conditions (Figure 2b). These results motivated us to synthesize a library of core-substituted derivatives and evaluate their catalytic potential within the previously established design framework for O-ATRP PCs, including absorption properties, excited-state characteristics, and redox properties.[7,15a] Seven dimethyl-dihydroacridine PCs with diverse electron-poor (cyanophenyl), electron-rich (methoxyphenyl), and highly conjugated (biphenyl or naphthalene) groups on both core and *N*-aryl positions were synthesized (Figure 2c). UV-vis spectroscopy was used to probe the ability to tune the frontier orbitals with various substitutions, and as such tune the absorption profiles of the PC (Figure 2b and Figures S41-S47).

Installation of electron-donating or -withdrawing groups onto the core-substituent was found to strongly influence $\lambda_{max,abs}$. For example, installation of 4-cyanophenyl groups (PC **3**, 382 nm) red-shifted $\lambda_{max,abs}$ by 42 nm compared to 4-methoxyphenyl groups (PC **2,** 340 nm) (Figure 2b). In a comparison of *N*-aryl modifications with biphenyl core substituents, decreasing *N*-aryl conjugation from a 1-naphthyl group (PCs **1** and **4**) to a phenyl group (PC **5**) led to a decrease in molar absorptivity (ε), (difference of ~18,000 $M^{-1}cm^{-1}$) but similar $\lambda_{max,abs}$ at 361 nm and 360 nm, respectively (Table 1, entries 1 and 4). Despite increasing pi-system conjugation through core-substitution, most PCs did not absorb beyond 400 nm. As an exception, the presence of 4-cyanophenyl groups at either core or *N*-aryl positions resulted in greater red-shifting of $\lambda_{max,abs}$, yielding some visible-light absorption. Notably, all the core-modified dimethyl-dihydroacridine PC candidates showed strong light absorption compared to non-core-modified **1a**, with ε ranging from 31,500 $M^{-1}cm^{-1}$ to 50,140 $M^{-1}cm^{-1}$. This high degree of efficiency in photoexcitation is also corroborated

through computationally predicted oscillator strengths (*f* values ranging from 1.211 to 1.749) indicating high π- π* transition probabilities (Table S2).

To study the nature of PC*, which governs alkyl bromide activation, a combination of DFT calculations and experimental studies were used to evaluate the ability of these PCs to access CT excited states, which have been empirically shown beneficial for good O-ATRP performance in structurally similar *N,N*-diaryl dihydrophenazine and *N*-aryl phenoxazine PCs.[24,15a] In these systems, electron density is transferred from the electron rich core to either the *N*-aryl or core-substituent, generating a shift in charge density within the molecule in its excited state, which is dictated by the electron accepting ability of the aryl "acceptor" as well as the environment surrounding the "donor" tricyclic core. The connection between PC CT and superior O-ATRP performance were investigated but with dissimilar conclusions. For *N*-aryl phenoxazines, increasing CT character has been shown to augment triplet yields, positing that higher concentrations of ^{3}PC* promotes fast activation.[26] Conversely, studies with *N,N*-diaryl dihydrophenazine PCs suggests that CT lowers *PC reduction potentials, slowing down activation, reducing radical concentrations, and minimizing termination.[15c]

Computationally, CT characteristics can be predicted through the presence of charge-separated singly occupied molecular orbitals (SOMOs) for ^{3}PC*. Of the PCs evaluated in this study, PCs **1**, **2,** and **7,** which possess either electron withdrawing groups or an extended π system as the *N*-aryl moiety, were predicted to have localization of the higher-lying SOMO onto the *N*-aryl substituent. PCs **4, 5,** and **6** all showed a higher-lying SOMO localization onto one core substituent, while PC **3** showed a higher-lying SOMO distributed across both core substituents (Figure S1).

Experimentally, CT character can be observed through a large Stokes shift and visualized through solvatochromism, where the polar ^{1}PC* is progressively stabilized by increasing solvent polarity, resulting in lower-energy emission and a corresponding red-shift in $\lambda_{max,em}$. Evaluation of CT from ^{1}PC* can estimate the CT character of ^{3}PC*, as CT singlet and triplet excited states are expected to be energetically degenerate, with low ΔE_{ST}.[23] A high fluorescence quantum yield (Φ_f) can indicate a lack of CT, as CT states have been shown to minimize fluorescence and increase triplet yields.[26] Consistent with previous observations in *N,N*-diaryl dihydrophenazine and *N*-aryl phenoxazine studies, for dimethyl-dihydroacridines subtle *N*-aryl substitution differences were found to be significant in influencing the nature of experimentally-observed CT character. Of these candidates, PCs **1** (Figure 2d), **2**, and **7** displayed the largest degree of CT through the largest measured Stokes shifts (ranging from 126 to 180 nm) paired with low Φ_f (0.1% to 8.7%), and the most dramatic solvatochromism spanning blue to yellow wavelengths of emission (Figure 2d and S1). By the same analysis, PCs **4** and **5** (Figure 2e and f) displayed a moderate degree of CT, while PCs **3** and **6** displayed the least amount of CT character (Figure S1). Notably, Φ_f values ranging from 0.1% (PC **2**) to 83% (PC **3**) can be obtained by modulating core-substitution.

Evaluation of excited-state redox potentials of these PCs was performed by DFT calculations to predict $E^{0*}_{T1,calc.}$ ($^{2}PC^{\bullet+}/^{3}PC^{*}$) values (Table 1). Experimentally, $E^{0*}_{S1,exp.}$ ($^{2}PC^{\bullet+}/^{1}PC^{*}$) was determined by a modified Rehm-Weller equation: $E^{0*}_{S1,exp.} = E_{1/2} -$

$E_{S1,exp.}$, where $E_{S1,exp.}$ was measured from the maximum wavelength of steady-state emission at room temperature. Experimental triplet energies ($E_{T1,exp.}$) were measured from PC phosphorescence at 77 K with a 1 ms gate-delay using time-resolved spectroscopy. $E_{S1,exp.}$ was also evaluated at 77 K with no gate delay, finding significant shifts in emission profiles. Interestingly, the PCs with the highest Stokes shifts, PCs **2** and **7** presented the lowest ΔE_{ST} values at 77 K (0.39 and 0.34 eV) (Table S4). Furthermore, computational E_{T1} predictions corresponded well with experimental values, with differences less than 0.07 eV.

Like absorption, the electronics of core-substitution strongly influenced $E^{0*}_{T1,exp.}$, where the PC with the lowest energy absorption (PC **3**) also possessed the lowest $E^{0*}_{T1,exp.}$ (−1.49 V vs. SCE). Correspondingly, PC **2,** with a relatively high energy absorption, was predicted to have the most reducing $E^{0*}_{T1,exp.}$ of −1.62 V vs SCE. Despite diverse absorption and CT properties, systematic study of various withdrawing, donating, and neutral *N*-aryl groups showed minimal influence on reduction potential, with $E^{0*}_{T1,exp.}$ ranging from −1.59 to −1.55 V vs. SCE.

The stability of the deactivating species $^2PC^{\bullet+}$ was measured by CV to determine $E_{1/2}$ ($^2PC^{\bullet+}/^1PC$), finding similar influence of the electronics of the core subsituent as was observed for both measured absorption characteristics and $E^{0*}_{T1,exp.}$ values. The presence of donating groups (PC **2**) resulted in stabilization of $^2PC^{\bullet+}$ ($E_{1/2}$ = 0.71 V vs SCE). Withdrawing groups (PC **3**) destabilized $^2PC^{\bullet+}$ and accessed a strongly oxidizing $^2PC^{\bullet+}$ ($E_{1/2}$ = 0.90 V vs. SCE). As in evaluation of $E^{0*}_{T1,exp.}$, the nature of the *N*-aryl group has minimal influence on $E_{1/2}$, with a range of 0.75 to 0.82 V vs. SCE. Computationally, the oxidizing ability of $^2PC^{\bullet+}$ (E^0_{ox}) was predicted by DFT, with values systematically ~0.25 V lower than the experimentally measured $E_{1/2}$, justifying the difference in magnitude between $E^{0*}_{T1,exp.}$ and $E^{0*}_{T1,calc.}$. In sum, the characterization of these dimethyl-dihydroacridine PC candidates shows that photophysical and electrochemical properties can be tuned in an analagous fashion to other established organic PCs with similar donor-acceptor motifs, while accessing more strongly oxidizing $^2PC^{\bullet+}$ characteristics and offering opportunities for previously unaccessable reactivity.

2. Application of Dimethyl-dihydroacridines to O-ATRP of Acrylate Monomers

To test the ability of these dimethyl-dihydroacridine PC candidates to catalyze O-ATRP of challenging acrylate monomers, initial polymerizations were conducted using *n*-butyl acrylate (BA) monomer, Diethyl 2-bromo-2-methylmalonate (DBMM) initiator, in *N,N*-dimethylacetamide (DMAc) solvent under 365 nm LED irradiation in batch reactor conditions. For comparison to dimethyl-dihydroacridine PCs, other well-studied organic PCs with diverse redox properties, including 3,7-di(4-biphenyl) 1-naphthalene-10-phenoxazine (**PhenO**), 5,10-di-(2-naphthyl)-5–10-dihydrophenazine (**PhenN**), and 1,2,3,5-tetrakis(carbazol-9-yl)-4,6-dicyanobenzene (**4Cz-IPN)** were applied in the O-ATRP of BA under the same reaction conditions. **PhenO** and **PhenN** both possess strongly reducing $E^{0*}_{T1,calc}$ (−1.70 and −2.12 V vs. SCE) and somewhat stabilized $E_{1/2}$ (0.65 and 0.21 V vs. SCE) while **4Cz-IPN** is a moderate reductant and strong oxidant (−1.06 and 1.50 V vs. SCE, respectively).[17f,7] In all cases these polymerizations were uncontrolled. For **4Cz-IPN**, M_n decreased over the course of polymerization from 170 kDa to 63 kDa, with $Đ > 2.0$ (Figure

S93). **PhenN** and **PhenO** showed some characteristics of an O-ATRP process, but suffered from non-linear growth of MW and high $Đ$ (Figures S91 and S92).

Initial application of PCs **1–7** to O-ATRP of BA supported that CT was required for good O-ATRP performance, similar to what was observed in *N,N*-diaryl dihydrophenazines.[24] For the PCs with the least amount of CT character (PCs **3** and **6**), the polymerization was uncontrolled, with MWs decreasing with increasing monomer conversion and $Đ > 2.0$. Excitingly, control over polymer MW growth, an indication of efficient deactivation processes, was realized for PCs **1**, **2**, **4**, **5**, and **7,** with all I^* values near 100% (Table 2, entries 1–7), where $I^* = (M_{n,GPC}/M_{n,\,theo.}) \times 100$. PC **2** provided the best results with $I^* =$ 96% at 77% conversion (Figure 4a), but produced a polymer with high $Đ$ at 1.53. For PCs **1, 2, 4, 5, and 7**, bimodal gel permeation chromatography (GPC) traces revealed an accompanying high MW p(BA) species present in low quantities. Control experiments with BA in DMAc under 365 nm irradiation revealed significant monomer autopolymerization (63% conversion at 2.5 hours) (Table S3) and thus likely contributed to the formation of this undesired high MW species.

As the best performing PC in these conditions (PC **2**) possessed the highest $E^{0*}_{T1,exp.}$ but also the lowest $E_{1/2}$, we hypothesized that promoting efficient activation could outcompete autopolymerization side-reactivity, leading to lower $Đ$ while maintaining control over MW growth. Notably, acrylate alkyl halide chain-end groups are more difficult to reduce compared to methacrylates, which can be observed by CV measurements of representative alkyl bromide initiators with methacrylate and acrylate functionalities. An acrylate analogue, methyl 2-bromopropionate, was found to undergo one-electron reduction at $E_{p/2} = -0.96$ V vs SCE, while a methacrylate model, methyl α-bromoisobutyrate, was reduced at $E_{p/2} = -0.80$ V vs. SCE, or a difference of 0.16 V (Figure S67), highlighting the need for high $E^{0*}_{T1,exp.}$ for efficient activation of acrylate-derived chain-end groups.

One alternative to batch reactor systems are continuous-flow reactors, which provide more uniform reaction irradiation and have been shown to improve photoinduced CRP systems through enhancing PC photoexcitation, thus promoting efficient alkyl bromide activation.[27] In this approach, a commercially available temperature-controlled Hepatochem PhotoRedOx box, an 18 W EvoluChem 365 nm LED, and a 2 mL PFA flow reactor was employed. Importantly, control experiments with BA in DMAc under these conditions did not produce any undesired autopolymerization (Table S14). PCs **1–7** were then evaluated for the O-ATRP of BA in continuous-flow, showing similar trends in performance as batch conditions, albeit with consistently lower $Đ$ (Table 2, entries 8–14). PC **2** again proved superior, however with initial high $Đ > 1.5$ at conversions < 50%, but lowered to 1.35 with $I^* = 97\%$ at 81% conversion.

Using PC **2,** further reaction optimization analyzing the effects of initiator, PC loading, and reaction concentration were conducted (Figures S124-S131). Increasing the DMF:BA ratio (1:1 to 1.5:1 v/v) significantly improved polymerization results, with $Đ < 1.5$ at all monomer conversions (Figure 4b). To further improve the system, the addition of various bromide salts was investigated, as this has been shown to promote deactivation in aqueous copper-catalyzed ATRP systems and in some photoredox-catalyzed ATRP systems.[28] Analysis of

LiBr, NaBr, KBr, and tetrabutylammonium bromide salts showed some decrease in $Đ$, with LiBr providing the greatest effect ($Đ \leq 1.23$) (Table S20). O-ATRP of BA using lithium salts with diverse anions (LiCl, LiI, $LiPF_6$) was also performed. A complete loss of MW control and $Đ > 2.0$ in all cases was observed (Table S20), illustrating the significance of the bromide anion in deactivation. Analysis of relative LiBr concentrations showed the conditions producing polymers with lowest $Đ$ (30 eq. LiBr relative to PC, or 83.3 mM) to also have the slowest overall reaction rate (Figure 4c and d), which paired with lower $Đ$, suggests LiBr concentration plays a key role in deactivation.

Next, a combination of DFT calculations and experimental studies were employed to explore the role of the LiBr salt in this O-ATRP system, probing its potential influence on both activation and deactivation mechanistic steps. One possibility is a Lewis-acid driven activation by Li^+ of the alkyl bromide ester polymer chain-end, facilitating rapid activation. However, CV revealed no change in reduction $E_{p/2}$ ($RX/RX^{\bullet -}$) of methyl-2-bromopropionate upon addition of LiBr ($E_{p/2} = -0.92$ V vs. SCE) (Figure S61). To evaluate potential effects of LiBr on PC photophysical behavior, PC **2** absorption and emission characterization was performed in the presence of LiBr, finding no changes in these properties (Figure S83 and S84).

Formally, the deactivation step is a termolecular process requiring low concentrations of $P_n^{\bullet}$, $^2PC^{\bullet +}$, and X^- to collide, which is entropically unfavorable. Previous studies with dihydrophenazines have shown that decreasing solvent polarity promotes ion-pairing of $^2PC^{\bullet +}X^-$, with a subsequent decrease in polymerization rate and improvement in performance.[24] As such, we propose that efficient deactivation requires oxidation of $P_n^{\bullet}$ by a $^2PC^{\bullet +}X^-$ ion-pair, which shifts a formal three-body collisional event to a more favorable pseudo-two-body event.[11,22a] In addition, we hypothesize a concerted mechanism for the oxidation of $P_n^{\bullet}$ by a $^2PC^{\bullet +}X^-$ ion-pair, where the formation of P_n-X is tied to the nuclear coordinate of X^- thus avoiding thermodynamically unfavorable carbocation P_n^+ intermediary species. Using DFT, the association of $^2PC^{\bullet +} + X^- \rightarrow {}^2PC^{\bullet +}X^-$ using PC **2** was predicted to be slightly endergonic ($\Delta G^0_{complex} = 0.6$ kcal/mol). As such, we postulate that the presence of excess bromide ions through LiBr addition increases the population of the proposed $^2PC^{\bullet +}X^-$ deactivator species, promoting rapid deactivation of the propagating chain-end and explaining the observed decrease in polymerization rates and lower $Đ$.

To further elucidate the relative importance of PC choice and the optimized reaction conditions in successful O-ATRP of acrylates, polymerizations were also conducted using **4-CzIPN**, **PhenO**, and **PhenN** in continuous-flow with LiBr additives. For **4Cz-IPN**, no polymerization was observed in the presence of LiBr, while O-ATRP without LiBr yielded an uncontrolled polymerization with Mn > 40 kDa and $Đ > 2.0$. (Table S21). The O-ATRP of BA using **PhenO** and **PhenN** was moderately improved under the optimized conditions, showing some control over molecular weight growth and with $Đ < 1.5$ at higher monomer conversions. However, both polymerizations displayed bimodal MW distributions by GPC, with I^* ranging from 31–109%.

Using these optimized conditions, MW control in the O-ATRP of BA catalyzed by PC **2** was demonstrated through adjustment of reaction stoichiometry, accessing MWs ranging from 2

to 26 kDa with $Đ < 1.36$ (Table 2, entries 1–5). However, targeting high MWs proved challenging, with $I^* > 100\%$, perhaps from a confluence of increased termination events and viscosity changes within the reactor. The O-ATRP of other alkyl and glycol acrylate monomers was performed using PC **2** with excellent control over MW and $Đ$ (Table 2, entries 7–11). O-ATRP of methyl methacrylate (MMA) was also accomplished, realizing low $Đ$ but with slightly bimodal GPC traces (Table 2, entry 12). As expected due to lower k_p, the O-ATRP of MMA was significantly slower than BA requiring 600 minutes of residence time for 72% monomer conversion, as compared to ~100 minutes for acrylates.

In batch conditions, no monomer conversion was observed using PC **2** under ambient atmosphere (Table S5). Recently, *N*-aryl phenoxazines were found to perform a well-controlled O-ATRP under ambient conditions when no vial headspace was present.[17e] To further test the oxygen-tolerance of dimethyl-dihydroacridines, the O-ATRP of BA was performed in optimized flow conditions using reagents and solvents previously exposed proceeded efficiently with no observed induction period, with $Đ \leq 1.24$ and I^* close to 100% (Table 3, entry 6).

To demonstrate the temporal control characteristic of an O-ATRP process, pulsed irradiation polymerization experiments were performed in batch conditions, showing no monomer conversion during dark periods with no irradiation (Figure S115). Analysis of bromide chain-end group retention of p(BA) was performed through MALDI mass spectrometry, revealing the presence of H-terminated and bimolecular radical termination products (Figure S161). Notably, no significant differences in chain-end groups between polymers synthesized with and without LiBr were observed (Figure S162).

To validate the chain-end group fidelity of the system and demonstrate the ability of this system to produce complex polymeric materials, chain-extensions were performed in continous-flow of an isolated p(*n*-BA) macroinitiator (M_n = 4.6 kDa, $Đ$ = 1.26) with ethyl acrylate (EA) to produce a block-copolymer p(*n*-BA)-*b*-p(EA) with $Đ$ = 1.16 (12 kDa). This polymer was then again reintroduced as a macroinitiator and further extended with *tert*-butyl acrylate to produce a well-defined triblock copolymer (M_n = 20 kDa, $Đ$ = 1.44) (Figure 5). An ^{1}H NMR spectrum for the p(*n*-BA) macroinitiator with detailed assignments (Figure S158) also shows the presence of α- and ω- chain-end groups.

Conclusion

In summary, we have reported the first successful O-ATRP of acrylate monomers with controlled MW and low $Đ$, enabled by rational design and development of a new family of dimethyl-dihydroacridine photocatalysts. Relationships between PC properties and catalytic performance are discussed, finding an interplay of photophysical and electrochemical properties is necessary to achieve the desired reactivity, as is supported by the best performing PC having the highest $E^{0*}_{T1,exp.}$ but the lowest $E_{1/2}$. A combination of reactor choice and LiBr additives is found to be significant in achieving a well-controlled system, which are proposed to promote the respective activation and deactivation steps of the O-ATRP cycle. We envision that dimethyl-dihydroacridines, with distinct properties and new reactivity, will further enable the advancement of organic photoredox catalysis in both small

molecule and macromolecular syntheses, aiding in the replacement of precious-metal catalysts for sustainable photoredox processes.

Supplementary Material

Refer to Web version on PubMed Central for supplementary material.

Acknowledgements

This work was supported by Colorado State University and the NIH (R35GM119702). This work used the Extreme Science and Engineering Discovery Environment (XSEDE), which is supported by National Science Foundation Grant ACI-1548562. C.-H. L. acknowledges a National Institutes of Health F32 Postdoctoral Fellowship (F32GM122392). The authors thank Dr. Matthew Ryan, Dr. Dianfeng Chen, and Max Kudisch for technical assistance and helpful discussions.

References

[1]. a) Romero NA, Nicewicz DA, Chem. Rev. 2016, 116, 10075–10166. [PubMed: 27285582] b) Prier CK, Rankic DA, MacMillan DWC, Chem. Rev. 2013, 113, 5322–5363. [PubMed: 23509883] c) Narayanam JMR, Stephenson CRJ, Chem. Soc. Rev. 2011, 40, 102–113. [PubMed: 20532341] d) Buzzetti L, Crisenza GEM, Melchiorre P, Angew. Chem. Int. Ed. 2019, 58, 3730–3747.e) Corrigan N, Shanmugam S, Xu J, Boyer C, Chem. Soc. Rev. 2016, 45, 6165–6212. [PubMed: 27819094]

[2]. a) Leibfarth FA, Mattson KM, Fors BP, Collins HA, Hawker CJ, Angew.Chem. Int. Ed. 2012, 52, 199–210.b) Chen M, Zhong M, Johnson JA, Chem. Rev. 2016, 116, 10167–10211. [PubMed: 26978484] c) Corrigan N, Yeow J, Judzewitsch P, Xu J, Boyer C, Angew. Chem. Int. Ed. 2019, 131, 5224–5243.

[3]. a) Matyjaszewski K, Adv. Mater. 2018, 30, 1706441.b) Ribelli TG, Lorandi F, Fantin M, Matyjaszewski K, Macromol. Rapid Commun, 2019, 40, 1800616.c) Ouchi M, Terashima T, Sawamoto M, Chem. Rev. 2009, 109, 4963–5050. [PubMed: 19788190]

[4]. a) Yang Q, Dumur F, Morlet-Savary F, Poly J, Lalevee J, Macromolecules 2015, 48, 1972–1980.b) Zhang G, Song IY, Ahn KH, Park T, Choi W, Macromolecules, 2011, 44, 7594–7599.c) Fors BP, Hawker CJ, Angewandte Chemie 2012, 51, 8850–8853. [PubMed: 22807122]

[5]. Shanmugam S, Boyer C, Science 2016, 352, 1053–1054 [PubMed: 27230364]

[6]. Yilmaz G, Yagci Y, Polym. Chem. 2018, 9, 1757–1762.

[7]. Theriot JC, McCarthy BG, Lim C-H, Miyake GM, Macromol. Rapid Commun. 2017, 38, 1700040.

[8]. Roth HG, Romero NA, Nicewicz DA, Synlett 2016, 27, 714–723.

[9]. a) Miyake GM, Theriot JC, Macromolecules 2014, 47, 8255–8261.b) Treat NJ, Sprafke H, Kramer JW, Clark PG, Barton BE, Alaniz JR, Fors BP, Hawker CJ, J. Am. Chem. Soc. 2014, 136, 16090–166101

[10]. a) Theriot JC, Lim C-H, Yang H, Ryan MD, Musgrave CB, Miyake GM, Science 2016, 352, 1082–1086. [PubMed: 27033549]

[11]. a) Pearson RM, Lim C-H, McCarthy BG, Musgrave CB, Miyake GM, J. Am. Chem. Soc. 2016, 138, 11399–11407. [PubMed: 27554292]

[12]. a) Singh VK, Yu C, Badgujar S, Kim Y, Kwon Y, Kim D, Lee J, Akhter T, Thangavel G, Park LS, Lee J, Nandajan PC, Wannemacher R, Milian-Medina B, Luer L, Kim KS, Gierschner J, Kwon MS, Nature Catalysis, 2018, 1, 794–804.b) Discekici EH, Anastasaki A, Read de Alaniz J, Hawker CJ, Macromolecules 2018 51, 7421–7434.

[13]. a) Narupai B, Page ZA, Treat NJ, McGrath AJ, Pester CW, Discekici EH, Dolinski ND, Meyers GF, Read de Alaniz J, Hawker CJ Angewandte Chemie 2018, 57, 13433–13438. [PubMed: 30155954] b) Discekici EH, Pester CW, Treat NJ, Lawrence J, Mattson KM, Narupai B, Toumayan EP, Luo Y, McGrath AJ, Clark PG, Read de Alaniz J, Hawker CJ ACS Macro Lett. 2016, 5, 258–262.

[14]. Pan X, Fang C, Fantin M, Malhotra N, So WY, Peteanu LA, Isse AA, Gennaro A, Liu P, Matyjaszewski K, J. Am. Chem. Soc. 2016, 138, 2411–2425. [PubMed: 26820243]

[15]. a) McCarthy BG, Pearson RM, Lim C-H, Sartor SM, Damrauer NH, Miyake GM, J. Am. Chem. Soc. 2018, 140, 5088–5101. [PubMed: 29513533] b) Cole JP, Federico CR, Lim C-H, Miyake GM, Macromolecules 2019, 52, 747–754. [PubMed: 30778265] c) Koyama D, Dale HJA, Orr-Ewing AJ, J. Am. Chem. Soc. 2018, 140, 1285–1293. [PubMed: 29300460]

[16]. a) Corbin DA, Lim C-H, Miyake GM, Aldrichimica Acta. 2019, 52, 7–21. [PubMed: 31839678]

[17]. a) Ryan MD, Pearson RM, French TA. Miyake GM, Macromolecules, 2017, 50, 4616–4622. [PubMed: 29551839] b) Ryan MD, Theriot JC, Lim C-H, Yang H, Lockwood AG, Garrison NG, Lincoln SR, Musgrave CB, Miyake GM, J. Polym. Sci. Part A: Polym. Chem. 2017, 55, 3017–3027.c) Ramsey BL, Pearson RM, Beck LR, Miyake GM, Macromolecules, 2017, 50, 28–2674.d) Buss BL, Beck LR, Miyake GM, Polym. Chem. 2018, 9, 1658–1665. [PubMed: 29628993] e) McCarthy B, Miyake GM, ACS Macro. Lett. 2018, 7, 1016–1021. [PubMed: 31827976] f) Du Y, Pearson RM, Lim C-H, Sartor SM, Ryan MD, Yang H, Damrauer NH, Miyake GM, Chem. Euro. J. 2017, 23, 10962–10968.g) Rao H, Lim C-H, Bonin J, Miyake GM, Robert M, J. Am. Chem. Soc. 2018, 140, 17830–17834. [PubMed: 30525556]

[18]. a) Pan X, Lamson M, Yan J, Matyjaszewski K, ACS Macro Lett. 2015, 4, 192–196.b) Chen D-F, Boyle BM, McCarthy BG, Lim CH, Miyake GM, J. Am. Chem. Soc. 2019, 141, 13268–13277. [PubMed: 31356063] c) Ramakers G, Krivkov A, Trouillet V, Welle A, Mobius H, Junkers T, Macromol. Rapid Commun. 2017, 38, 1700423.

[19]. Destarac M, Polym. Chem. 2018, 9, 4947–4967.

[20]. Beuermann S, Buback M, Prog. Polym. Sci. 2002, 27, 191–254.

[21]. Anastasaki A, Nikolaou V, Zhang Q, Burns J, Samanta SR, Waldron C, Haddleton AJ, McHale R, Fox D, Percec V, Wilson P, Haddleton DM, J. Am. Chem. Soc. 2014, 136, 1141–1149. [PubMed: 24372509]

[22]. Treat NJ, Fors BP, Kramer JW, Christianson M, Chiu C-Y, Read de Alaniz J, Hawker CJ, ACS Macro. Lett. 2014, 3, 580–584.

[23]. Wong MY, Zysman-Colman E, Advanced Materials 2017, 29, 1605444.Li W, Li B, Cai X, Gan L, Xu Z, Li W, Liu K, Chen D, Su S-J, Angew. Chem. Int. Ed. 2019, 58, 11301–11305.

[24]. Lim C-H, Ryan MD, McCarthy BG, Theriot JC, Sartor SM, Damrauer NH, Musgrave CB, Miyake GM, J. Am. Chem. Soc. 2017, 139, 348–355. [PubMed: 27973788]

[25]. Arias-Rotondo DM, McCusker JK, Chem. Soc. Rev. 2016, 45, 5803–5820. [PubMed: 27711624]

[26]. Sartor SM, McCarthy BG, Pearson RM, Miyake JM, Damrauer NH, J. Am. Chem. Soc. 2018, 140, 4778–4781. [PubMed: 29595966]

[27]. a) Hartman RL, McMullen JP, Jenson KF, Angew. Chem. Int. Ed. 2011, 50, 7502–7519.b) Buss BL, Miyake GM, Chem. Mater. 2018, 30, 3931–3942. [PubMed: 30559577] c) Junkers T, Wenn B, React. Chem. Eng. 2016, 1, 60.d) Tucker JW, Zhang Y, Jamison TF, Stephenson CRJ, Angew. Chem. Int. Ed. 2012, 51, 4144–4147.

[28]. a) Simakova A, Averick SE, Konkolewicz D, Matyjaszewski K, Macromolecules 2012, 45, 6371–6379.b) Fantin M, Isse AA, Gennaro A, Matyjaszewski K, Macromolecules, 2015, 48, 6862–6875.

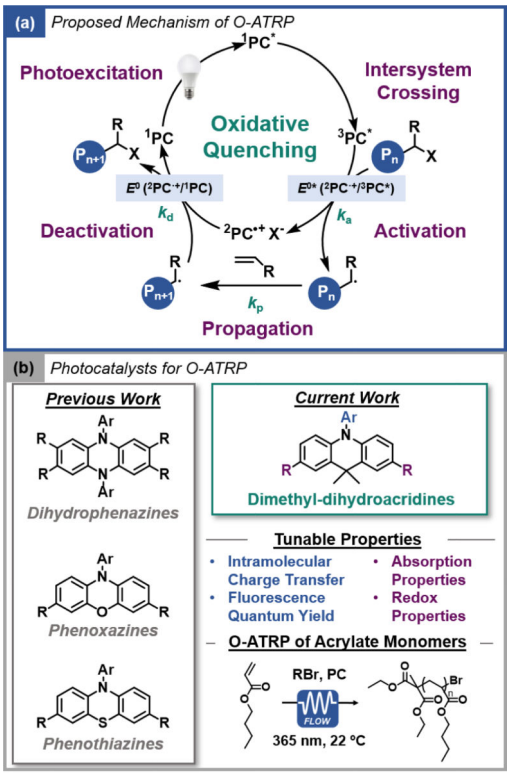

Figure 1.

(a) Proposed mechanism of O-ATRP. b) Previously reported PCs developed for O-ATRP (left) with the new dimethyl-dihydroacridine PC family investigated in this work (right).

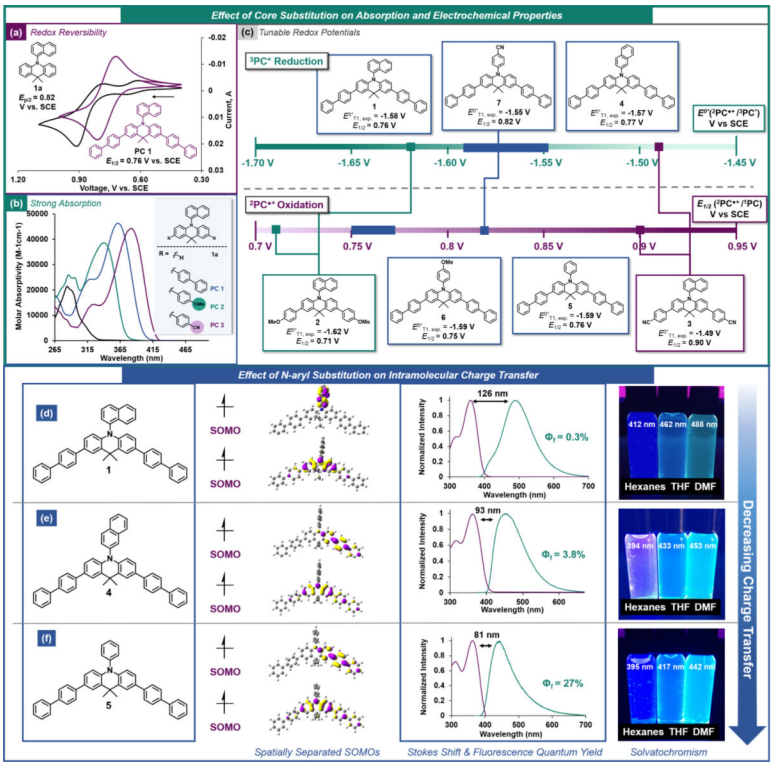

Figure 2.

(a) Cyclic voltammogram of PC **1a** and PC **1**. (b) UV-vis spectrum of PCs **1a**, **1, 2, and 3**. (c) Electrochemical series of experimentally-measured excited state redox potentials $E^{0*}_{T1,\,exp.} = E^{0}(^{2}PC^{\bullet+}/^{3}PC^{*})$ and oxidation potentials $E_{1/2}$ ($^{2}PC^{\bullet+}/^{1}PC$) of PCs investigated in this study. High- and low-lying SOMO for PCs with electronically neutral *N*-aryl groups, overlays of the absorption profiles (purple) and emission profiles (teal) with the experimentally determined Stokes shifts for each PC, and photographs of the PCs dissolved in solvents with increasing polarity with $\lambda_{max,emission}$ for each solvent for PC **1** (d), **4** (e), and **5** (f). All CV, UV-vis, and emission data collected in *N,N*-dimethylformamide. See SI for full experimental and computational details.

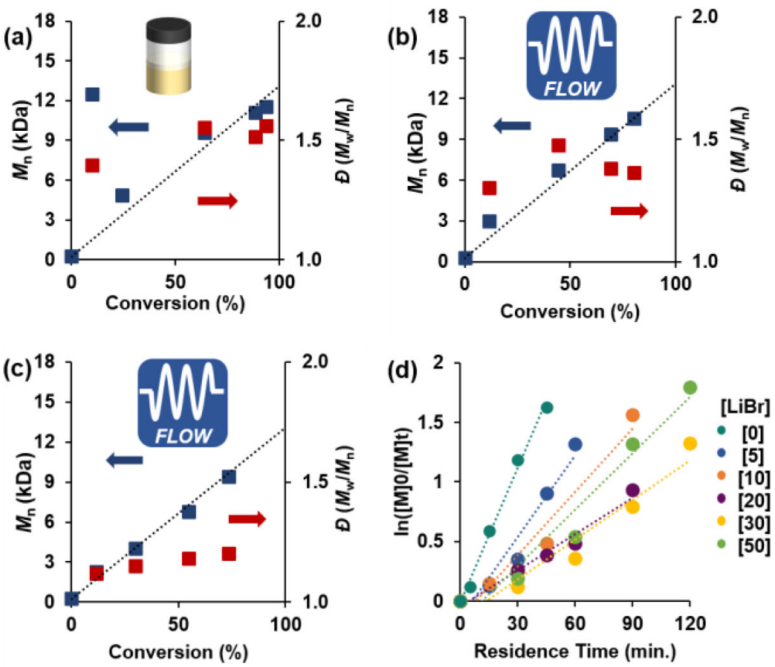

Figure 4.

(a) Plots of M_n vs. conversion (blue) and $Đ$ vs. conversion (red) for O-ATRP of BA plotted against the theoretical M_n (dashed line) using PC 2 conducted in batch reactor, (b) flow reactor, and (c) flow reactor with 30 eq. LiBr relative to PC. (d) First order kinetic plot of O-ATRP of BA with varying LiBr eq. relative to PC. Conditions are [1000]:[10]:[1]:[x] of [BA]:[DBMM]:[PC 2]:[LiBr] with 1.0 eq. by volume of DMAc for (a) and 1.5 eq. for (b) and (c), and irradiated by 365 nm LEDs.

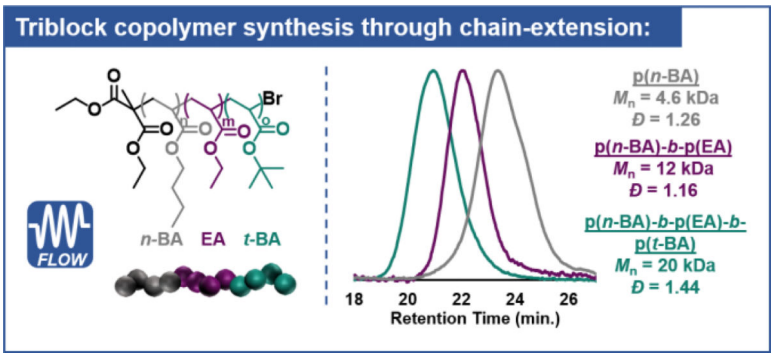

Figure 5:

Results of sequential chain-extension experiments with corresponding GPC traces to produce a p(*n*-BA)-*b*-p(EA)-*b*-p(*t*-BA) triblock copolymer.

Table 1.

Summary of photophysical and electrochemical measurements for PCs 1–7.

PC	$\lambda_{max,abs}$.(nm)[a]	ε ($M^{-1}cm^{-1}$)	$\lambda_{max,S1\ em.}$ (nm)[b]	Φ_f (%)	$E_{S1,exp.}$ (eV)[c]	$E_{T1,calc.}$ (eV)[d]	$E_{T1,77\ K}$ (eV)[c,e]	$E_{1/2}$ ($^2PC^{\bullet+}/^1PC$) (V vs. SCE)[f]	$E^{0*}_{S1,exp.}$ ($^2PC^{\bullet+}/^1PC^*$) (V vs. SCE)[g]	$E^{0*}_{T1,exp.\ 77\ K}$ ($^2PC^{\bullet+}/^3PC^*$) (V vs. SCE)[e,g]	$E^{0*}_{T1,calc.}$ ($^2PC^{\bullet+}/^3PC^*$) (V vs. SCE)[d]
1	361	46,300	487	0.3	2.55	2.41	2.34	0.76	−1.79	−1.58	−1.86
2	340	38,600	509	0.1	2.44	2.36	2.33	0.71	−1.73	−1.62	−1.94
3	382	44,300	458	83	2.71	2.43	2.39	0.90	−1.81	−1.49	−1.69
4	360	49,800	453	3.8	2.74	2.30	2.34	0.77	−1.98	−1.57	−1.77
5	361	31,500	443	27	2.80	2.29	2.35	0.76	−2.04	−1.59	−1.75
6	363	43,100	444	70	2.79	2.28	2.34	0.75	−2.04	−1.59	−1.78
7	355	50,100	535	8.2	2.32	2.39	2.37	0.82	−1.50	−1.55	−1.78

[a] Absorption wavelength measured using ultraviolet-visible spectroscopy in DMF.

[b] Emission wavelength measured using steady-state fluorescence spectroscopy in DMF.

[c] Energies were calculated using the maximum wavelength of emission.

[d] DFT calculations performed at uM06/6–311+Gdp/uM06/6–31+Gdp level of theory with CPCM-described solvation in aqueous solvent.

[e] Spectral emission measured at 77 K after 1 ms gate-delay.

[f] All measurements were performed in a 3-compartment electrochemical cell with an $Ag/AgNO_3$ reference electrode in MeCN (0.01 M) and 0.1 M NBu_4PF_6 electrolyte solution with DMF analyte solution. Platinum was used at the working and counter electrodes.

[g] Excited-state redox potentials were calculated using energies estimated from the maximum wavelength of singlet or triplet emission and the experimentally measured $E_{1/2}$; $E^{0*}_{S1,exp.} = E_{1/2} - E_{S1,exp.}$ and $E^{0*}_{T1,\ exp.\ 77K} = E_{1/2} - E_{T1,77K}$.

Table 2:

Summary of results of O-ATRP of BA performed in batch and flow using PCs 1–7[a]

Entry	PC	Reactor	Conv. (%)[b]	$M_{n,calc,}$ (kDa)[c]	$Đ$ (M_w/M_n)[c]	I^* (%)[d]
1	1	Batch	65	9.3	1.64	92
2	2	Batch	77	10.6	1.53	96
3	3	Batch	42	31.4	4.93	35
4	4	Batch	68	9.6	1.62	93
5	5	Batch	59	8.7	1.70	90
6	6	Batch	72	25.8	3.52	37
7	7	Batch	76	10.9	1.89	92
8	1	Flow	67	8.9	1.59	100
9	2	Flow	81	11.0	1.35	97
10	3	Flow	71	13.1	4.57	72
11	4	Flow	81	11.1	1.48	96
12	5	Flow	79	10.2	1.48	102
13	6	Flow	82	11.4	3.58	94
14	7	Flow	73	9.6	1.54	100

[a] Conditions are [1000]:[10]:[1] of [BA]:[DBMM]:[PC] with 1.0 eq. DMAc to BA by volume and irradiated by 365 nm LEDs. Batch reactions are conducted under ambient temperatures and flow reactions at 22 ºC.

[b] Determined by ^{1}H NMR.

[c] Measured using GPC.

[d] Calculated by (Conv. × [Mon]/[RX] × $M_{w,Mon}$)/1000.

[e] Initiator efficiency (I^*) calculated by (Theo. M_n/Calc. M_n) × 100.

Table 3:

Summary of results of O-ATRP of acrylate monomers performed using PC 2.[a]

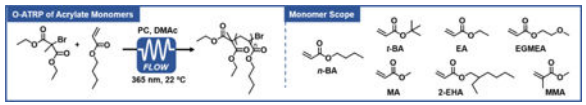

Entry	Monomer	[Monomer]:[DBMM]	Res. Time (min.)	Conv. (%)	$M_{n,calc}$, (kDa)	$M_{w,calc}$, (kDa)	$Đ$ (M_w/M_n)	I* (%)
1	*n*-BA	[1000]:[2.5]	90	89	26.4	45.7	1.35	173
2	*n*-BA	[1000]:[5]	120	88	15.2	22.8	1.32	150
3	*n*-BA	[1000]:[10]	120	73	9.4	9.7	1.20	103
4	*n*-BA	[1000]:[20]	180	80	7.3	5.4	1.19	74
5	*n*-BA	[1000]:[40]	180	67	5.4	2.4	1.18	44
6[b]	*n*-BA	[1000]:[10]	120	85	10.3	11.1	1.24	108
7	*t*-BA	[1000]:[10]	120	92	13.8	12.1	1.23	88
8	MA	[1000]:[10]	90	92	10.0	8.1	1.30	81
9	EA	[1000]:[10]	90	76	7.5	7.8	1.19	105
10	2-EHA	[1000]:[10]	90	90	16.3	16.8	1.53	104
11	EGMEA	[1000]:[10]	60	92	10.5	12.3	1.37	117
12	MMA	[1000]:[10]	600	72	8.8	7.4	1.17	85

[a]Conditions are [1000]:[×]:[1]:[30] of [monomer]:[DBMM]:[PC 2]:[LiBr] with 1.5 mL DMAc relative to 1 mL monomer performed in continuous-flow and irradiated by 18 W 365 nm LED at 22 °C.

[b]Reaction components sparged with air for 30 minutes before polymerization. See SI for full experimental details.